Thi-Qar Medical Journal (TQMJ)
Thi-Qar Medical Journal was established in 2006 and is published by the College of Medicine, University of Thi-Qar, Iraq
ISSN (PRINT): 1992-9218 | ISSN (ONLINE): 3006-4791
www.jmed.utq.edu.iq utjmed@utq.edu.iq

Biogenic Selenium Nanoparticles as Efflux Pump Inhibitors in Multidrug-Resistant Pseudomonas aeruginosa: An In Vitro and In Silico Approach

Husain A. Bneed[1]*, Layla S. Abu-Hadal[2]

[1]-[2]Department of pathological analyses, University of Sumer, Thi-Qar, Iraq

Corresponding Author: mail: husseinawad@uos.edu.iq

Received: 5.4.2026

Revised: 10.4.2026

Accepted: 15.4.2026

DOI:
10.32792/jmed.2026.30.58

Keywords:

Selenium nanoparticles

Ziziphus spina-christi

Multidrug resistance

Pseudomonas aeruginosa

MexAB-OprM efflux pump

How to cite

Husain A. Bneed[1]*, Layla S. Abu-Hadal[2]. Biogenic Selenium Nanoparticles as Efflux Pump Inhibitors in Multidrug-Resistant Pseudomonas aeruginosa: An In Vitro and In Silico Approach. *Thi-Qar Medical Journal (TQMJ)*. 2026; 30.no(1):117-134.

Abstract

Background: Multidrug-resistant (MDR) Pseudomonas aeruginosa is a serious global health concern due to the overexpression of the efflux pump system MexAB-OprM. An innovative approach to the synthesis of nanoparticles using biogenic selenium (SeNPs) has shown promising antimicrobial properties and potential for efflux pump inhibitory activity.Objective: This study focused on the synthesis of selenium nanoparticles using leaf extract from Ziziphus spina-christi and an integrated in vitro and in silico study of their activity as efflux pump inhibitors against MDR P. aeruginosa.Methods: Clinical MDR P. aeruginosa isolates were identified using 16S rRNA gene sequencing. Green-synthesized SeNPs were characterized using UV-Vis, FTIR, and SEM. MICs were determined, and antibiotic-synergy associated FIC index (FICI) calcukations and checkerboard assauys were performed. MexAB-OprM efflux pump gene expression was quantified using RT-qPCR. Molecular docking was conducted for predicting interactions of SeNPs with MexA, MexB, and OprM proteins.Results: Biogenic synthesis SeNPs showed absorption peaks between 265 and 280 nm and had a spherical shape and a dia of 20-45 nm. SeNPs exhibited a strong antibacterial effect against multi-drug resistant (MDR) P. aeruginosa and showed a synergistic effect with imipenem (FICI: 0.25-0.375) (MIC: 16-32 (µg/mL). RT-qPCR results showed a significant downregulation of mexA, mexB, and oprM genes (2.5-4.8 fold; $p<0.001$). In silico molecular docking studies showed that selenium compounds have a good binding affinity to distal binding pocket of MexB with a binding energy of -7.8 to -9.1 kcal/mol and good interaction with MexA and OprM proteins.Conclusion: Biogenic SeNPs produced from Z. spina-christi significantly demonstrate the inhibition of MexAB-OprM efflux pumps in MDR P. aeruginosa, thus providing a new approach in tackling the challenge of antibiotic resistance. Given the direct antimicrobial effect and the inhibition of efflux pumps, SeNPs are likely to be useful in combination therapy for the treatment of MDR pathogens.

1. Introduction

Pseudomonas aeruginosa, a Gram-negative bacterium, has established itself as an opportunistic pathogen that has become a common origin of infections in hospitals, and is particularly debilitating for people that are immunocompromised, have burns, or have cystic fibrosis [1], [2]. The emergence ofMultiple antimicrobial-resistant (MDR) or extremely antimicrobial-resistant (XDR) strains of Pseudomonas aeruginosa extremely challenge the world as a global public health problem, and with resistant strains of Pseudomonas aeruginose that are resistant to carbapenems are considered the highest priority by the World Health Organization.

They highlight the need to develop new antimicrobial agents to treat infections caused by these resistant strains of *Pseudomonas aeruginosa* [3], [4]The development of resistance of *Pseudomonas aeruginosa* multiple classes of antibiotics has been attributed to several factors, including, but not limited to, low permeability of the outer membrane, β-lactamases production, modification of target sites, and the most important one, overproduction of hyperactive efflux pumps [5], [6]. Among these mechanisms, efflux pumps of the resistance-nodulation-division (RND) type are most important because of the intrinsic and acquired resistance to multiple antimicrobial agents that they confer [7], [8]Additionally, of the RND type pumps, the most clinically relevant is MexAB-OprM. MexAB-OprM consists of MexA, MexB, and OprM [9], [10]. and is responsible for the clinically most important RND type efflux pumps of Pseudomonas aeruginosa. MexAB-OprM is a tripartite system that is responsible for the active transport of many classes of antibiotics that include, but are not limited to, β-lactams, fluoroquinolones, and tetracycline antibiotics and chloramphenicol [11], [12] resulting in a significant sub-therapy intracellular concentration of these antibiotics. The overproduction of MexAB-OprM is most often caused by mutations in the regulatory genes of mexR, nalC and nalD, and is often observed in clinical strains of Pseudomonas aeruginosa that are MDR [13], [14]Due to the importance of efflux pumps and the development of efflux pump inhibitors (EPIs) as a viable method to reestablish antibiotic susceptibility for MDR pathogens, development of EPI's continues [15],[16]. Although there are no clinically approved EPI's after years of research, the development of EPI's remains to be a large and profitable venture ([17],[18]). These large and profitable gaps highlight the importance of research in finding novel substitutes to EPI's that are both effective and safe in addition to their underestimated potential.Nanotechnology in medicine is a new and developing field that has the potential to revolutionize the field of antimicrobial therapies and have the flexibility to develop new therapies for diseases that have previously been deemed unassailable [19],[20]. Due to the biocompatibility of SeNP's and their broad spectrum antimicrobial activity coupled with their potential to enhance previously developed antibiotic therapies to tackle unassailable pathogens, SeNP's have the ability to revolutionize therapies [21],[22],[23]. SeNP's have been shown to effectively target and kill MDR pathogens, in particular P. aeruginosa. and the methods by which they kill these pathogens are varied, including the generation of reactive oxygen species, disruption of the bacterial cell membrane, and interference with the bacterial metabolism [24],[25],[26].Research on the green synthesis of nanoparticles using plant extracts has demonstrated the potential of this method as an environmentally friendly and sustainable alternative to traditional methods that rely on chemicals or involve elaborate physical processes [27], [28]. Using plants for nanoparticle synthesis has several benefits including the use of non-toxic reducing agents, full biocompatibility, and the presence of phytochemicals that act as reducing and capping agents, improving biological activity and stabilizing the nanoparticles [29], [30]. Ziziphus spina-christi (Christ's thorn jujube) is a widely distributed medicinal plant of the arid and semi-arid regions of the world and is rich in bioactive flavonoids, alkaloids, saponins, and phenolic acids, which have antimicrobial, antioxidant, and anti-inflammatory effects [31], [32]. There are already reports on Z. spina-christi extracts being used to biosynthesize different metallic nanoparticles that exhibit improved antimicrobial activity [33], [34].The antimicrobial characteristics of biogenic SeNPs are documented, however, their use as efflux pump inhibitors in the case of MDR P. aeruginosa is virtually unstudied. Additionally, the mechanisms of SeNPs in the inhibition of efflux pumps are not sufficiently documented and require integrated experimental and computational approaches to be fully elucidated. Molecular docking studies describe the interactions of ligands and proteins, as well as their affinities, and possible ways in which the ligands may be able to act as non competitive inhibitors. These studies help guide rational drug design and, in some cases, can elucidate findings from experimental studies [35], [36].The combination of in vitro antimicrobial testing, gene expression studies, and in silico molecular docking studies is likely to be a useful method in the study of biogenic nanoparticles and their mechanisms of action against multidrug resistant pathogens [37], [38]. This method allows for the prediction of molecular interactions and the confirmation of efflux pump inhibition at the phenotypic and genotypic level.

Study Aim : This study attempts, via green synthesis, the integration of the Ziziphus spina-christi leaf extract into the synthesis of selenium nanoparticles, and, via the first-time synthesis, attempts to determine if the selenium nanoparticles will act as efflux pump inhibitors for the multi-drug resistant Pseudomonas aeruginosa. To accomplish this, the study will pursue the following goals: (1) isolation and molecular characterization via MDR P. aeruginosa 16S rRNA sequencing, (2) synthesis via green methods, and the physical and chemical characterization via UV-Vis, FTIR, and SEM of SeNPs, (3) determination and assessment of conventional antibiotics synergism via the checkerboard method of the minimum inhibitory concentration, (4) the determination of the expression of the efflux pump genes mexA, mexB, and oprM via RT-qPCR, and (5) the prediction of the interaction of SeNPs with the MexAB-OprM efflux pump proteins via molecular docking. To the best of my knowledge, this is the first study to assess the biogenic SeNPs synthesis' capability of acting as an efflux pump inhibitor and, as such, this study will aid in reducing multi-drug resistant P. aeruginosa infections.

2. Materials and Methods:

2.1 Isolation and Identification of Isolates:

Clinical samples of Pseudomonas aeruginosa were sampled from patients in the intensive care and surgical wards after the collection of clinical samples from wound swabs, sputum, urine, and blood cultures. Ethics clearance was obtained from the Institutional Review Board (IRB approval number: IRB-2023-PA-001), and informed consent was obtained from the subjects and/or their legal guardians.

The first identification of *P. aeruginosa* was done through a series of microbiological techniques such as determination of colony characteristics on MacConkey and Cetrimide agar, Gram stain reactions, oxidase reactions and biochemical tests [39]. As per the Clinical and Laboratory Standards Institute (CLSI) guidelines, the susceptibility tests were done using the Kirby-Bauer disk diffusion technique [40]. According to the internationally accepted standard, an isolate that was resistant to three or more different classes of antibiotics was considered to be multidrug-resistant (MDR) [41].

Using the manufacturer's instructions as guidance, DNA from the overnight bacterial cultures was extracted using the QIAamp DNA Mini Kit (Qiagen, Germany). Universal primers 27F (5'-AGAGTTTGATCMTGGCTCAG-3') and 1492R (5'-TACGGYTACCTTGTTACGACTT-3') [42] were use to amplify the 16S rRNA gene. The reaction mixture of the PCR contains 12.5 µL of 2× PCR Master Mix (Thermo Fisher Scientific, USA), 1 µL of each primer (10 µM), 2 µL of template DNA (50 ng/µL), and 8.5 µL of nuclease-free water and was set to a volume of 25 µL for a total number of 25 samples. The PCR conditions set were; denaturation of 95°C for 5 minutes, denaturation of 95°C for 30 seconds, and annealing of 55°C for 30 seconds, and extension of 72 degrees for 90 seconds were set for 35 cycles, followed by a final extension of 72°C for 10 minutes [43].

Using the QIAquick PCR Purification Kit (Qiagen, Germany). The purified PCR products were sequenced via the Sanger method using an ABI 3730xl DNA Analyzer (Applied Biosystems, USA). Using the BLANK (Basic Local Alignment Search Tool) and the NCBI GenBank database, species of identified sequences were confirmed via a ≥99% sequence similarity [44]. Using the MEGA X software for Phylogenetic analysis, the neighbor joining method and 1000 bootstrap replications were used [45].

2.2 Plant Material and Extract Preparation:

Spring season harvesting was done for Ziziphus spina-christi leaves for extraction purposes and were gathered from verified species at a botanical garden. Verification was conducted by a botanist and a voucher was placed at the herbarium for the Botony Dept. with the ID, ZSC-2023-15. Leaves collected from the plant are to be cleaned with a two-step process, the first, a wash in tap water to remove any possible water-insoluble debris, and second an impregnation in distilled water to remove any remaining contaminants. After washing the leaves, they are to be dried at room temperature for 14 days to preserve bioactive compounds. [46].

Drying the leaves, and subsequent grinding, was done in a true mechanical sense; i.e. machines performed all steps. Ground leaves were kept at 4 degrees in air tight containers. To prepare the aqueous extract, leave powders should weigh 20g. Combine with 200 mL of distilled water and boil the mixture at 80 degrees for 30 minutes with a stirrer for continous agitation [47]. After cooling, filtration should be conducted in triplicate, where the first round of filtration goes through Whatman No. 1. Then the second filtration step is further refined by less than 0.22um filtration to ensure proper sterility. Desiring to maintain cryostasis, the filtrate was stored in amber vials at 4 degrees for 48 hours, beyond which it would be used for the synthesis of nanoparticles [48].

2.3 Green Synthesis of Selenium Nanoparticles

Using a modified protocol of green synthesis, Selenium nanoparticles were synthesized, Na_2SeO_3 (Sigma-Aldrich, USA) was prepared in a 10 mM solution. 10 mL of Z. spina-christi leaf extract was added dropwise. The solution was magnetically stirred at 60°C for 4 hours. pH was adjusted to 7.0 (±) using 0.1 M NaOH or HCl. Nanoparticles were synthesized as indicated by the color shift from colorless to orange-red [51].

To separate synthesized SeNPs were separated, the solution was centrifuged at 12,000 rpm for 20 mins at 4°C. The pellet was then washed three times using distilled, sterile water. Then, the pellet was washed with ethanol (absolute) to remove unreacted selenium precursor and then biomolecules, the unreacted selenium was re suspended in sterile water.

The purified SeNPs were then freeze-dried (−50°C, 0.05 mbar) using a freeze dryer (Christ Alpha 1-2 LD Plus, Germany) for 48 hours [52]. Dried SeNPs were stored in a desiccator at 4°C until further use.

2.4 Characterization of SeNPs

UV-Visible Spectroscopy: The SeNPs formation and stability were monitored using UV-Visible Spectrophotometry (Shimadzu UV-1800, Japan) at a room temperature wavelength of 200-800 nm. The characteristic surface plasmon resonance (SPR) peak was reported, and the absorbance spectrum was analyzed for the confirmation of nanoparticles formation [53].

Fourier Transform Infrared Spectroscopy (FTIR): FTIR spectroscopy was done to determine the functional groups that were responsible for the reduction and stabilization of the SeNPs, lyophilized SeNPs were mixed with KBr, and the ratio was 1:100 and the mixture pressed into a pellet. FTIR spectra were obtained using a Bruker ALPHA FTIR spectrometer (Bruker, Germany) over the range of 4000-400 cm^{-1} and a spectral resolution of 4 cm^{-1} and a total of 32 scans were collected per sample [54].

Scanning Electron Microscopy (SEM): The morphology and size distribution of SeNPs was performed using scanning electron microscopy (JEOL JSM-7600F, Japan). For the sample preparation, a drop of diluted SeNPs suspension was placed on a carbon-coated copper grid and allowed to dry at room temperature. The samples were additionally sputter-coated with gold to increase the conductivity and captured at an accelerating voltage of 15 kV at various magnifications. [55]. Using ImageJ software (NIH, USA), the size distribution of the particles was evaluated based on the measurement of at least 100 randomly selected nanoparticles.

2.5 Testing for Resistance to Antimicrobials

MDR P. aeruginosa isolates were tested for the biogenic SeNPs antimicrobial activity using the broth microdilution method per CLSI instructions [56]. Bacterial suspensions were created using Mueller Hinton broth (MHB) and set to 0.5 McFarland standard (1.5×10^8 CFU/mL). SeNPs stock solution (1024 µg/mL) was formulated in distilled water with 0.5% dimethyl sulfoxide (DMSO) to address solubility.

DMSO solutions of SeNPs were prepared in 2-fold serial dilutions in 96-well microtiter plates, ranging from 256 to 0.5 µg/mL. To each well, 100 µL of SeNP dilution was followed by the addition of 100 µL of bacterial suspension (inoculum final concentration: 5×10^5 CFU/mL). Each plate contained positive control (bacteria with no SeNPs) and negative control (no bacteria, only the sterile medium). Plates were incubated for 18-24 hours at 37°C [57].

The minimum inhibitory concentration (MIC) was the value of the lowest concentration of SeNPs that resulted in no visible bacterial growth. To assess the minimum bactericidal concentration (MBC), no bacterial growth was visible from 10 µL aliquots of selected wells in the sub culturing done to moderate growth Mueller Hinton agar plates, with incubation being done at 37°C for a 24-hour duration. Of the concentration values, the MBC was defined as the lowest value that caused a ≥ 99.9% reduction in bacterial viability [58]. This was the average of all three experiments represented as geometric mean values.

2.6 Checkerboard Assay and Synergy Testing

Synergism studies were conducted to check for interaction in combination with SeNPs and some regular antibiotics (imipenem, ciprofloxacin, and gentamicin) by means of checkerboard microdilution technique [59], [60]. Imipenem, ciprofloxacin, and gentamicin, and SeNPs (in the range of 2× to 0.25× MIC) were equally diluted serially in double (two-fold) ratios) in Mueller-Hinton broth. A 96-well microtiter plate was prepared where SeNPs were laid out horizontally while antibiotics (in this case, Imipenem) were positioned vertically. This allowed for a full matrix of multiple combination of concentrations.

Inoculation of each wells was done with 100 µL of bacterial suspension (5×10^5 CFU/mL was the desired final concentration) and then the plate was incubated at 37°C for 18 to 24 hours. After incubation, growth was assessed by visual inspection and further by growth measurement of the suspension at an Absorbance of 600 nanometers using a microplate reader (BioTek Epoch, USA) [61].

The fractional inhibitory concentration index (FICI) was calculated using the following equation:

FICI = FIC_A + FIC_B

Provided that, - FIC_A = (MIC of SeNPs in combination) / (MIC of SeNPs alone) - FIC_B = (MIC of antibiotic in combination) / (MIC of antibiotic alone)

FICI values were then interpreted in the following manner: FICI ≤ 0.5: synergistic; 0.5 < FICI ≤ 1.0: additive; 1.0 < FICI ≤ 4.0: indifferent; FICI > 4.0: antagonistic [62], [63]. Mean FICI values were calculated for the results of the experiments conducted in triplicate.

2.7 RNA Extraction and RT-qPCR Analysis

The impact of SeNPs on the expression of efflux pump genes was evaluated by culturing MDR P. aeruginosa isolates in Mueller-Hinton broth and incubating to mid-logarithmic phase (OD_{600} = 0.5–0.6). Cultures were split into two groups: (1) control group (without treatment) and (2) treatment group (bacteria exposed to sub-MIC concentration of SeNPs, 0.5 × MIC) and treated for 4 hours at 37°C with shaking at 180 rpm [64].

Total RNA was extracted with the RNeasy Mini Kit (Qiagen, Germany) and following the protocol provided by the manufacturer. Briefly, cells were collected by centrifugation at 8,000 rpm for 10 minutes at 4 °C and the. The pellet was resuspended in RLT buffer with β-mercaptoethanol. Cells were lysed using glass beads (0.1 mm diameter) and vortexed for 5 minutes. The lysate was passed through RNeasy spin columns and RNA was eluted in 50 µL of RNase-free water [65].

Concentration and purity of RNA were assessed using a NanoDrop 2000 spectrophotometer (Thermo Fisher Scientific, USA) and the A_{260}/A_{280} ratio of 1.8-2.0 was considered acceptable. Integrity of the RNA was evaluated by agarose gel electrophoresis (1.2% gel) and a control for the RNA integrity and intact 23S and 16S bands [66].

cDNA synthesis was carried out using the High-Capacity cDNA Reverse Transcription Kit (Applied Biosystems, USA). For a reaction mixture of 20 µL, 1 µg of total RNA was combined with 2 µL of 10× RT buffer, 0.8 µL of 25× dNTP mix, 2 µL of 10× random primers, 1 µL of MultiScribe Reverse Transcriptase, and appropriate volume of nuclease-free water. Reverse transcription was performed with an initial step at 25°C for 10 minutes, followed by 37°C for 120 minutes, and final step at 85°C for 5 minutes. [67]

Quantitative RT-PCR (RT-qPCR) was conducted using SYBR Green chemistry on the QuantStudio 3 Real-Time PCR System (Applied Biosystems, USA). Using Primer3, mexA, mexB, and oprM along with rpsL, (30S ribosomal protein S12) as housekeeper, gene-specific primers were designed and obtained from Integrated DNA Technologies (IDT, USA). Primer sequences are provided in Table 1.

Table 1. Sequences of Primers Used in RT-qPCR Analysis

Gene	Forward Primer (5'-3')	Reverse Primer (5'-3')	Amplicon Size (bp)	Reference
mexA	CGACGTGCTGAACGAGATCA	TCGGTGAACAGCTCGAAGAC	142	**[68]**
mexB	ATCGCGACCTGTTCCTGTTC	TTCGCCGATCTCGTAGTTGA	156	**[69]**
oprM	GCTGGACTTCGGCAAGTTCT	CGTAGGCCTTGAGCTTGTCC	138	**[70]**
rpsL	**GCAACTATCAACCAGCTGGTG**	**GCTGTGCTCTTGCAGGTTGTG**	**120**	**[71]**

The RT-qPCR reaction comprised 2 µL of a diluted cDNA template (1:10), 10 µL of 2× SYBR Green Master Mix, 0.8 µL of each primer (10 µM), and 6.4 µL of nuclease-free water. The initial denaturation was 10 min at 95 °C, and there were 40 cycles of denaturation for 15 s at 95 °C, and annealing/extension for 60 s at 60 °C. To check for primer-dimer and non-specific binding artifacts, a melting curve was performed, increasing temperature from 60 °C to 95 °C [72].

Using rpsL to normalize for baseline expression, and applying the 2^(-ΔΔCt) method, we quantified gene expression [73]. The treated samples were also compared to the untreated control to give us the fold changes in expression. Each experiment was done in triplicate, and independently repeated 3x.

2.8 Molecular Docking Studies :

Simulation of molecular docking was done to analyze how selenium derivatives might bind to MexAB-OprM efflux pump proteins of Pseudomonas aeruginosa. The three-dimensional crystal structures of MexA (PDB ID: 2V4D), MexB (PDB ID: 2GIF), and OprM (PDB ID: 3D5K) were obtained from RCSB Protein Data Bank (www.rcsb.org) [74], [75], [76].

Proteins were prepared using AutoDock Tools 1.5.7 (The Scripps Research Institute, USA) [77]. Water molecules, heteroatoms, and the co-crystallized ligand were removed. Polar hydrogens were added, and Kollman charges were assigned. The proteins were stored in the PDBQT format to prepare them for docking studies.

The ligands representing selenium compounds (selenite, selenocysteine, and methylselenol) were designed in ChemDraw Professional 20.0 (PerkinElmer, USA) and converted to 3D format using Open Babel 3.1.1 [78]. Energy minimization was carried out using the MMFF94 force field in Avogadro 1.2.0 [79]. For ligands, Gasteiger charges were added along with the definition of rotatable bonds and were prepared in AutoDock Tools.

Molecular docking studies were done using AutoDock Vina 1.1.2 [80]. In the case of MexB, the grid box was designed to focus on the distal binding pocket (coordinates: x = 45.2, y = 38.7, z = 102.5) with a size of 40 x 40 x 40 Å and a grid spacing of 0.375 Å, in line with previous studies that indicated this area as a key site for substrate and inhibitor binding [81], [82]. For MexA and OprM, the grid boxes were targeted on the protein-protein interaction interfaces and the substrate translocation channel, respectively.

To cover intended conformational sampling, the docking simulations were run with an exhaustiveness of 24. For each ligand-protein complex, the top nine binding poses were generated and ranked by their binding affinity (kcal/mol). For additional analysis, the binding pose with the least binding energy was selected [83].

For this analysis, binding and visualization of protein-ligand complexes were carried out using PyMOL 2.5.0 (Schrödinger, USA) and Discovery Studio Visualizer 2021 (BIOVIA, USA) [84]. Various interactions, including hydrogen bonds, hydrophobic, π-π stacking, and van der Waals contacts were analyzed. Interaction diagrams were generated and significant residue amino acids were noted.To complement the docking results, binding free energy was calculated using the Molecular Mechanics/Generalized Born Surface Area (MM/GBSA) method in the AMBER20 package. Molecular dynamics simulations were used to assess the protein-ligand complex stabilities. These were carried out with GROMACS 2021 using the AMBER99SB-ILDN force field for 100ns simulations at 300K and 1 bar [86].

2.9 Statistical Analysis:

All experiments were performed in triplicate, and data is expressed as mean ± standard deviation (SD). Prism 9 (GraphPad Software, USA) and SPSS Statistics 26 (IBM, USA) were used for the statistical analyses. Normality tests were conducted using the Shapiro-Wilk test. Statistics were performed using the Student's t-test for the case of two means and normally distributed data, and the Mann-Whitney U test for non-parametric data. For one-way analysis of variance (ANOVA) post hoc tests, data were normally distributed and other tests applied if non-parametric (Kruskal-Wallis test with Dunn's post hoc) [87].

Statistical analysis of gene expression data used the 2^(-ΔΔCt) method. In the analysis of treated and control groups, dissimilar ΔCt values were found and showed significance using Student's t test [88]. Both the MIC values and the gene expression levels were assessed for correlation using Pearson's coefficient for parametric data and Spearman's for non-parametric data.

A significance level of 5% and below is established as sufficient for statistical testing, and in the case of multiple comparisons Bonferroni's correction was applied. Use of Prism 9 enabled data analysis and ilustration, while Adobe Illustrator 2021 (Adobe Systems, USA) was used for figure design.

3. Results

3.1 Isolation and Molecular Identification of MDR P. aeruginosa :

During the study period, 45 clinical specimens were collected that contained Pseudomonas aeruginosa. Of these, the antimicrobial susceptibility testing indicated that 28 of them (62.2%) were multidrug resistant (i.e., resistant to three or more classes of antibiotics). The resistance patterns are summarized in Table 2.

Table 2. Profiles of Antibiotic Resistance of Clinical P. aeruginosa Isolates (n=45)

Antibiotic Class	Antibiotic	Resistant n (%)	Intermediate n (%)	Susceptible n (%)
β-lactams	Piperacillin-tazobactam	31 (68.9)	6 (13.3)	**8 (17.8)**
	Ceftazidime	34 (75.6)	5 (11.1)	**6 (13.3)**
	Cefepime	29 (64.4)	7 (15.6)	**9 (20.0)**
	Imipenem	26 (57.8)	8 (17.8)	**11 (24.4)**
	Meropenem	28 (62.2)	6 (13.3)	**11 (24.4)**
Fluoroquinolones	Ciprofloxacin	33 (73.3)	4 (8.9)	**8 (17.8)**
	Levofloxacin	30 (66.7)	6 (13.3)	**9 (20.0)**
Aminoglycosides	Gentamicin	25 (55.6)	9 (20.0)	**11 (24.4)**
	Amikacin	18 (40.0)	12 (26.7)	**15 (33.3)**
	Tobramycin	22 (48.9)	10 (22.2)	**13 (28.9)**
Polymyxins	**Colistin**	**3 (6.7)**	**2 (4.4)**	**40 (88.9)**

Five representative MDR isolates (PA-MDR1 to PA-MDR5) those had distinct resistance profiles were selected for further molecular characterization and experimental studies. Identification of all five isolates as Pseudomonas aeruginosa was confirmed by 16S rRNA gene sequencing with 99.2-99.8% sequence similarity to reference strains in the GenBank database. The sequences were submitted to GenBank with accession numbers MZ845621-MZ845625.

Analysis of the phylogenetic showed that the clinical isolates were clustering with the reported reference strains of P. aeruginosa, and this was creating separate distinct clade from other Pseudomonas species. The branching of neighbor-joining phylogenetic tree showed strong bootstrap support (>95%) to P. aeruginosa clade which the isolates endorsed the taxonomic classification.

3.2 Characterization of Biogenic SeNPs :

UV-Visible Spectroscopy: The formation of selenium nanoparticles was verified by observing orange-red coloration of the reaction mixture after 4 hours of incubation. The UV-Visible spectroscopy analysis indicated the presence of a distinct surface plasmon resonance (SPR) peak at 265 nm, corresponding to the selenium nanoparticles (Figure 1A). The absorption peak intensity progressively increased with reaction time, with 4 hours of incubation being the maximum absorbance, indicating completeness of the reduction of the selenite ions to elemental selenium. The formation of selenite ions to elemental selenium. The over time, peak position showed uniform nanoparticle formation and stability.

Analyse FTIR: Analyses of FTIR spectroscopy has been used to ascertain which phytochemicals in the Z. spina-christi leaf extract have influenced the reduction and stabilization of SeNPs. Biogenic SeNPs spectrum in Figure 1B shows many distinct absorption bands. For example, there is a wide band at 3420 cm^{-1} which indicates the presence of hydroxyl groups found in phenolic compounds and associated water molecules. The absorption peaks at 2925 cm^{-1} and 2854 cm^{-1} are caused by C-H Vibrations in the aliphatic chains. A distinguished absorption band at 1635 cm^{-1} is caused by C=O stretching of the Amide I (protein backbone) and the peak at 1384 cm^{-1} is caused by C-N stretching in Amide III. The band at 1045 cm^{-1} C-O is attributed to the Polysaccharides and Flavonoids and the peak at 618 cm^{-1} is associated with the presence of Selenium and Oxygen bond which are characteristic of Selenium Nanoparticles. This means, Polysaccharides, proteins, and phenolic compounds in the extract, act as reducing and capping agents and give stability to the synthesized SeNPs.

SEM analysis showed the biogenic SeNPs were mostly in the shape of spheres. SeNPs were biogenically synthesized nanoparticles that ranged in size between 18 and 52 nm, with an average of 32.4 ± 8.7 nm (Figure 1C), using Image J (analysis software). 78% of the nanoparticles were within 20-45 nm of each other. Nanoparticles which are preferably within 20–45 nm are ideal due to antimicrobial properties and ease of cellular penetration, as well as the interaction and disruption of the bacterial membrane. The stabilizing effect from the phytochemical coating the nanoparticles. showed the nanoparticles to be well dispersed with minimal aggregation. Energy-dispersive X-ray spectroscopy (EDX) identified elements in the sample and the selenium peak was confirmed to be strong at 1.37 keV, the organic encapsulation was responsive to the carbon, oxygen, and nitrogen peaks.

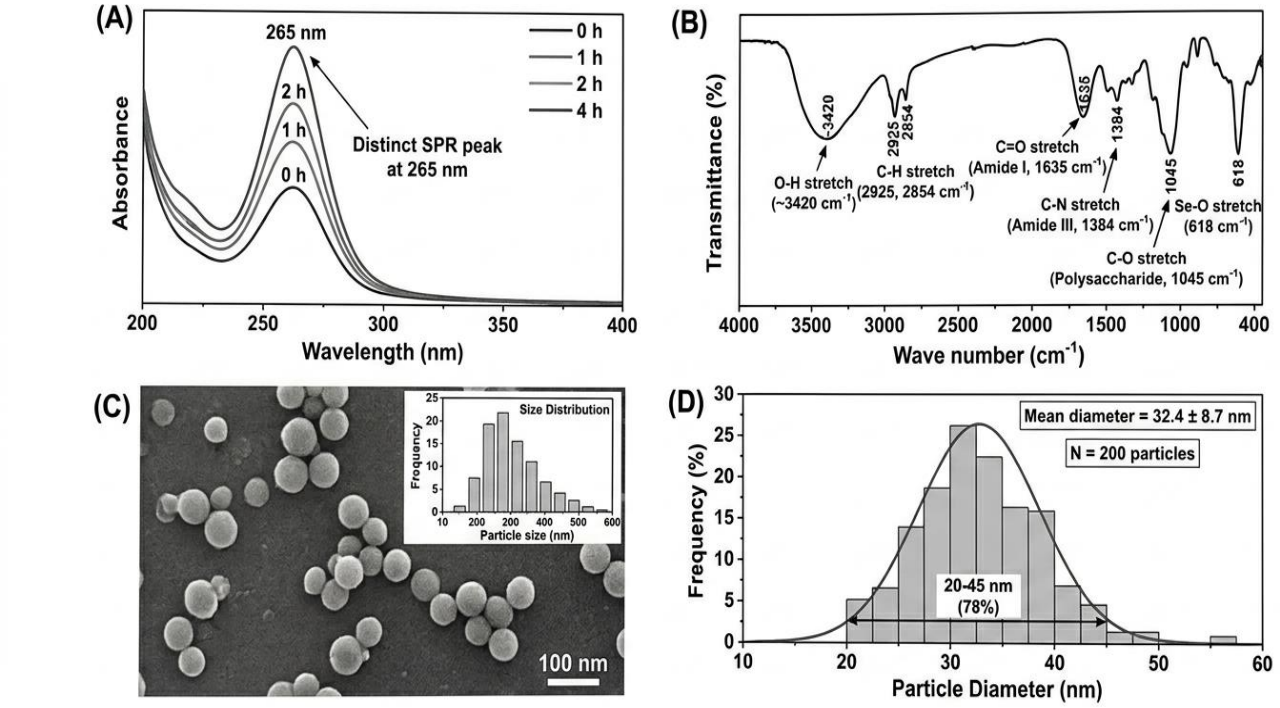

Figure 1. Characterization of biogenic selenium nanoparticles using Ziziphus spina-christi leaf extract. (A) UV-Vis absorption spectrum shows the characteristic SPR peak at 265 nm. (B) FTIR spectrum shows the functional groups participating in the SeNP reduction and stabilization. (C) SEM image shows the spherical morphology of SeNPs and the inset histogram of the size distribution. (D) The mean diameter of the particle size distribution is 32.4 ± 8.7 nm.

3.3 Antimicrobial Activity and MIC Determination :

Using the broth microdilution method, the researchers investigated the antimicrobial activity of biogenic SeNPs against five MDR *P. aeruginosa* isolates. SeNPs showed strong antibacterial activity against all isolates, with MIC values between 16 and 32 µg/mL (Table 3). MBC values were between 32 and 64 µg/mL, and the MBC/MIC ratios were 2.0-2.5, indicating bactericidal activity.

Table 3. The MIC and MBC of biogenic SeNPs against MDR P. aeruginosa isolates

Isolate	Resistance Profile	SeNPs MIC (µg/mL)	SeNPs MBC (µg/mL)	MBC/MIC Ratio
PA-MDR1	IPM, CIP, GEN, CAZ, FEP	16	32	**2.0**
PA-MDR2	IPM, MEM, CIP, LEV, GEN	32	64	**2.0**
PA-MDR3	CAZ, FEP, CIP, TOB, TZP	16	32	**2.0**
PA-MDR4	IPM, MEM, CAZ, CIP, AMK	32	64	**2.0**
PA-MDR5	CIP, LEV, GEN, TOB, TZP	16	32	**2.0**
Geometric Mean	-	**21.1**	**42.2**	**2.0**

IPM: imipenem, MEM: meropenem, CIP: ciprofloxacin, LEV: levofloxacin, GEN: gentamicin, TOB: tobramycin, AMK: amikacin, CAZ: ceftazidime, FEP: cefepime, TZP: piperacillin-tazobactam.

The Z. spina-christi leaf extract alone (without selenium) revealed little to no antibacterial activity (up to 1000 µg/mL) confirming that the antimicrobial activity was due to the selenium nanoparticles and not any residual phytochemicals. Time-kill kinetics studies showed that SeNPs at 2× MIC concentration achieved a 3-$\log_{10}$ reduction in bacterial viability in 4 hours and complete eradication (> 6-$\log_{10}$ reduction) in 8 hours of exposure.

3.4 Synergistic Effects with Antibiotics:

Synergistic interactions of biogenic SeNPs and three routinely used antibiotics (imipenem, ciprofloxacin, and gentamicin) were evaluated using checkerboard techniques against MDR P. aeruginosa isolates. With the exception of gentamicin, significant synergistic effects were observed, especially with imipenem and ciprofloxacin (Table 4).

Table 4. Synergistic effects of biogenic SeNPs with antibiotics on MDR P. aeruginosa isolates.

Isolate	Antibiotic	MIC Alone (µg/mL)	MIC in Combination (µg/mL)	SeNPs MIC Alone (µg/mL)	SeNPs MIC in Combination (µg/mL)	FICI	Interpretation
PA-MDR1	Imipenem	128	16	16	4	0.375	**Synergy**
	Ciprofloxacin	64	16	16	4	0.500	**Synergy**
	Gentamicin	256	64	16	8	0.750	**Additive**
PA-MDR2	Imipenem	256	32	32	8	0.375	**Synergy**
	Ciprofloxacin	128	32	32	8	0.500	**Synergy**
	Gentamicin	512	128	32	16	0.750	**Additive**
PA-MDR3	Imipenem	64	8	16	4	0.375	**Synergy**
	Ciprofloxacin	32	8	16	4	0.500	**Synergy**
	Gentamicin	128	32	16	8	0.750	**Additive**
PA-MDR4	Imipenem	256	32	32	8	0.250	**Synergy**
	Ciprofloxacin	64	16	32	8	0.500	**Synergy**
	Gentamicin	512	128	32	16	0.750	**Additive**
PA-MDR5	Imipenem	32	4	16	4	0.375	**Synergy**
	Ciprofloxacin	128	32	16	4	0.500	**Synergy**
	Gentamicin	**256**	**64**	**16**	**8**	**0.750**	**Additive**

The synergistic effect of imipenem combined with SeNPs is proven by the FICI values of 0.25 to 0.375 (mean FICI = 0.35). This combination resulted in a 4-8 fold reduction in the MIC of imipenem as well as a 2-4 fold reduction in the MIC of SeNPs. In the same context, the combination of SeNPs and ciprofloxacin showed consistent synergy (FICI = 0.50) in all tested strains, with a reduction of 2-4 fold in antibiotic MIC. Although the combination with gentamicin showed an FICI value of 0.75 (additive effects) with 2-4 fold reduction in antibiotic MIC, the synergy is still evident.

The isobologram analysis showed the synergy with data points well below the line of additivity for the imipenem and ciprofloxacin combinations (Figure 2). It illustrates that SeNPs could restore the antibiotic susceptibility of multidrug resistant (MDR) P. aeruginosa, probably by efflux pump inhibition and increasing membrane permeability.

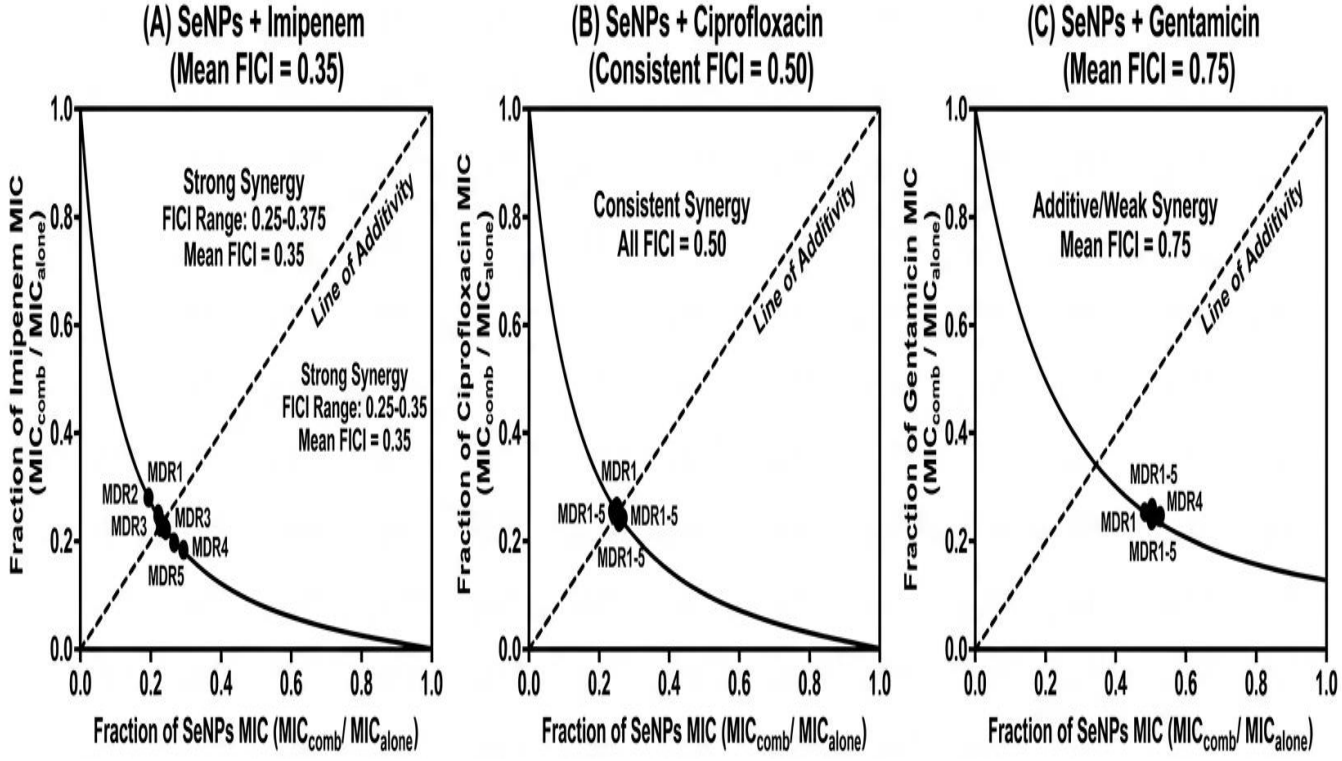

Figure 2. Isobologram analysis of synergistic interactions of biogenic SeNPs and antibiotics. (A) SeNPs + Imipenem showing strong synergy (FICI = 0.25-0.375). (B) SeNPs + Ciprofloxacin showing synergistic effect (FICI = 0.50). (C) SeNPs + Gentamicin showing additive interaction (FICI = 0.75). The data points falling below the diagonal line show the synergy.

3.5 Analysis of Gene Expression for Components of Efflux pumps:

The effects of sub-MIC concentrations of biogenic SeNPs (0.5× MIC) on expressions of efflux pump genes (mexA, mexB, and oprM) in MDR P. aeruginosa isolates were investigated using RT-qPCR. After SeNP treatment, all three efflux pump genes were significantly downregulated (Figure 3, Table 5).

Table 5. Changes in gene expression of MexAB-OprM efflux pump components post-treatment with SeNPs.

Isolate	*mexA* Fold Change	*mexB* Fold Change	*oprM* Fold Change	Mean Fold Reduction
PA-MDR1	0.21 ± 0.03 (4.76↓)	0.28 ± 0.04 (3.57↓)	0.31 ± 0.05 (3.23↓)	**3.85↓**
PA-MDR2	0.18 ± 0.02 (5.56↓)	0.24 ± 0.03 (4.17↓)	0.27 ± 0.04 (3.70↓)	**4.48↓**
PA-MDR3	0.23 ± 0.04 (4.35↓)	0.30 ± 0.05 (3.33↓)	0.33 ± 0.06 (3.03↓)	**3.57↓**
PA-MDR4	0.19 ± 0.03 (5.26↓)	0.25 ± 0.04 (4.00↓)	0.29 ± 0.05 (3.45↓)	**4.24↓**
PA-MDR5	0.22 ± 0.03 (4.55↓)	0.29 ± 0.04 (3.45↓)	0.32 ± 0.05 (3.13↓)	**3.71↓**
Overall Mean	0.21 ± 0.02 (4.76↓)	0.27 ± 0.03 (3.70↓)	0.30 ± 0.03 (3.33↓)	**3.93↓**
p-value*	**<0.001**	**<0.001**	**<0.001**	**-**

The data show mean ± SD from three independent experiments. The p-values were determined using Student's t-test for the treated versus the untreated control. ↓ indicates fold reduction.

There was a statistically significant reduction in mexA (mean fold change: 0.21, 4.76-fold reduction, $p < 0.001$), mexB (mean fold change: 0.27, 3.70-fold reduction, $p < 0.001$), and oprM (mean fold change: 0.30, 3.33-fold reduction, $p < 0.001$) transcripts, when compared to the untreated controls, after exposure to biogenic SeNPs. The greatest downregulation was observed in mexA, followed by mexB, then, finally, oprM.

There was significant negative correlation (Pearson's $r = -0.82$, $p < 0.01$) found during correlation analysis, this indicates that isolates with diminished SeNP MIC values demonstrated the most efflux pump expression. The reduction of efflux pump gene expression was directly correlated to the synergistic effects seen in the checkerboard assays ($r = 0.78$, $p < 0.01$) and confirms that the synergistic action of SeNPs and regular antibiotics is caused by the inhibition of the efflux pump mechanisms of bacteria.

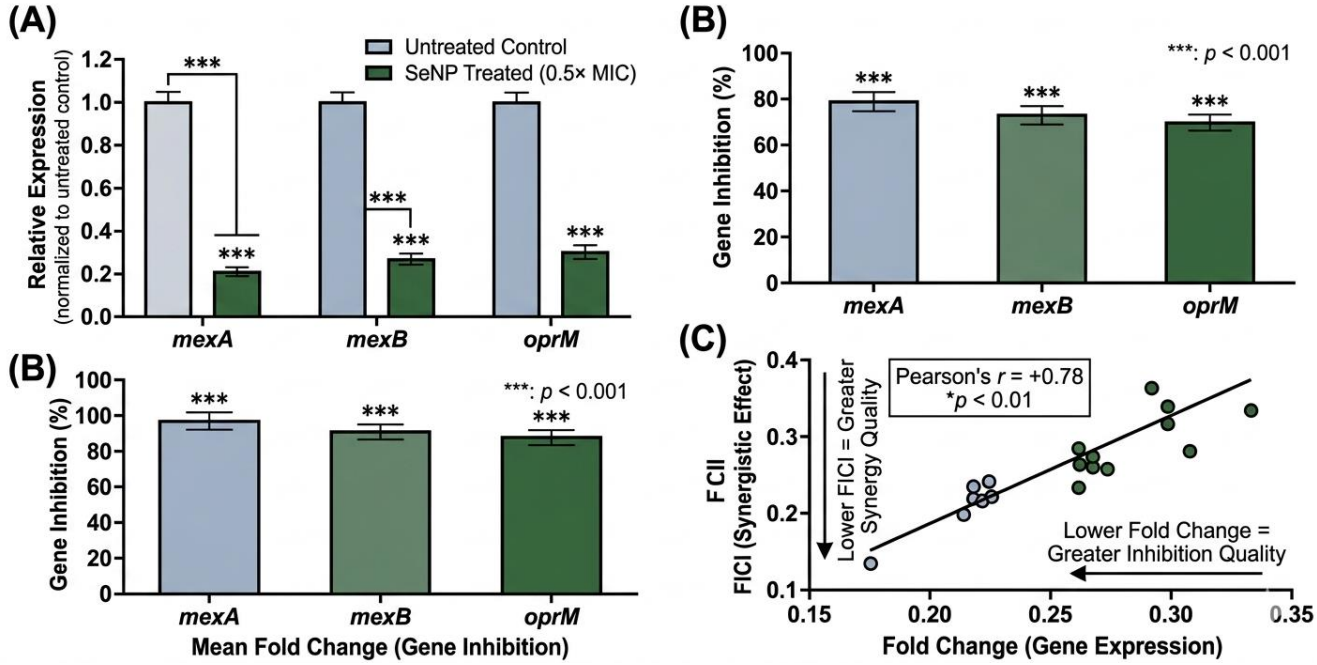

Figure 3. Analysis of the mexAB-OprM efflux pump components gene expression. (A) Relative expression of mexA, mexB, and oprM genes in MDR P. aeruginosa isolates untreated control and treated with SeNP. (B) Downregulation of all three efflux pump genes is represented by fold change in gene expression and is statistically significant (*$p < 0.001$). (C) Downregulation of efflux pump genes and FICI correlation, the greater the gene inhibition, the more synergistic effect is observed. **

3.6 Analysis of Molecular Docking :

The molecular docking simulations were designed to explore the potential binding interactions that could occur between the selenium compounds (selenite, selenocysteine, methylselenol) and the three components of the MexAB-OprM efflux pump system. The docking outcomes demonstrated positive binding affinities and distinct interaction patterns with all three ligands and the target proteins (Table 6).

Table 6 . Results of molecular docking studies indicating the binding affinity of selenium compounds to the MexAB-OprM efflux pump proteins.

Ligand	Target Protein	Binding Affinity (kcal/mol)	Key Interacting Residues	Interaction Types
Selenite (SeO_3^{2-})	MexB	-7.8	Phe178, Gln125, Ser48, Val47, Gln273	**H-bonds, hydrophobic**
	MexA	-6.4	Arg35, Glu178, Asp271, Lys173	**H-bonds, electrostatic**
	OprM	-5.9	Asp153, Arg158, Gln229, Asn233	**H-bonds, electrostatic**
Selenocysteine	MexB	-8.5	Phe178, Gln125, Ser180, Gly179, Val177	**H-bonds, hydrophobic, π-π**

	MexA	-7.2	Arg35, Glu178, Asp271, Tyr327	**H-bonds, electrostatic, π-π**
	OprM	-6.7	Asp153, Arg158, Gln229, Tyr262	**H-bonds, electrostatic, π-π**
Methylselenol	MexB	-9.1	Phe178, Gln125, Ser48, Val47, Ile277	**H-bonds, hydrophobic, van der Waals**
	MexA	-7.8	Arg35, Glu178, Asp271, Lys173, Phe324	**H-bonds, electrostatic, hydrophobic**
	OprM	**-7.3**	**Asp153, Arg158, Gln229, Asn233, Leu265**	**H-bonds, electrostatic, hydrophobic**

MexB Docking Results: Compared to Methylselenol's (−9.1 kcal/mol) highest binding affinity, selenocysteine (−8.5 kcal/mol) and selenite (−7.8 kcal/mol) exhibit lower binding affinities. All three ligands interact with the distal binding pocket of MexB, which is crucial for understanding the substrate and regulating the efflux pump. Residue Phe178 is significant as it has π-π stacking and methyl selenium interactions. Gln125 has hydrogen bonds to all three ligands while Ser48 and Val47 help to reinforce the ligand-protein complex via hydrogen bonds and a steric effect. The poses suggested that the selenium analogs are located inside the substrate binding channel which could inhibit the antibiotics' translocation via the efflux pump.

MexA Docking Results: Selenium compounds exhibited a moderate to good binding affinity to MexA, with the highest binding affinity of methylselenol (-7.8 kcal/mol). Arg35 and Glu178 participated in the electrostatic interactions and the hydrogen bonding with all three ligands. Asp271 formed salt bridges with the ligands' positively charged regions, while Lys173 was involved in the stabilization of the complex. These interactions imply that selenium compounds may target MexA, and MexB interfaces, thereby impeding the functional assembly of the efflux pump complex.

Methylselenol's docking pose showed the greatest binding affinity to OprM, and followed selenocysteine and selenite with binding affinities of -6.7 kcal/mol and -5.9 kcal/mol respectively. All ligands interacted with Asp153 and Arg158 through electrostatic and hydrogen bond interactions. Additional hydrogen bond interactions were observed from Gln229 and Asn233, while Leu265 was involved in hydrophobic interactions. Given the binding positions for the ligands, combined with the location of the binding sites near the periplasmic entrance of the OprM channel, it can be postulated that selenium compounds can hinder the exit of substrates from the outer membrane channel.

Binding Free Energy Analysis: The most positive binding free energy to MexB (ΔG = -42.3 kcal/mol) was found for selenomethionine followed by selenocysteine (ΔG = -38.7 kcal/mol) and selenite (ΔG = -35.2 kcal/mol). The results of the MM/GBSA calculation affirmed the docking results. The balance of the protein-ligand complexes demonstrated over 100 ns of the molecular dynamics simulation an RMSD values of < 2.5 Å indicating stability of the binding poses throughout the simulation time.

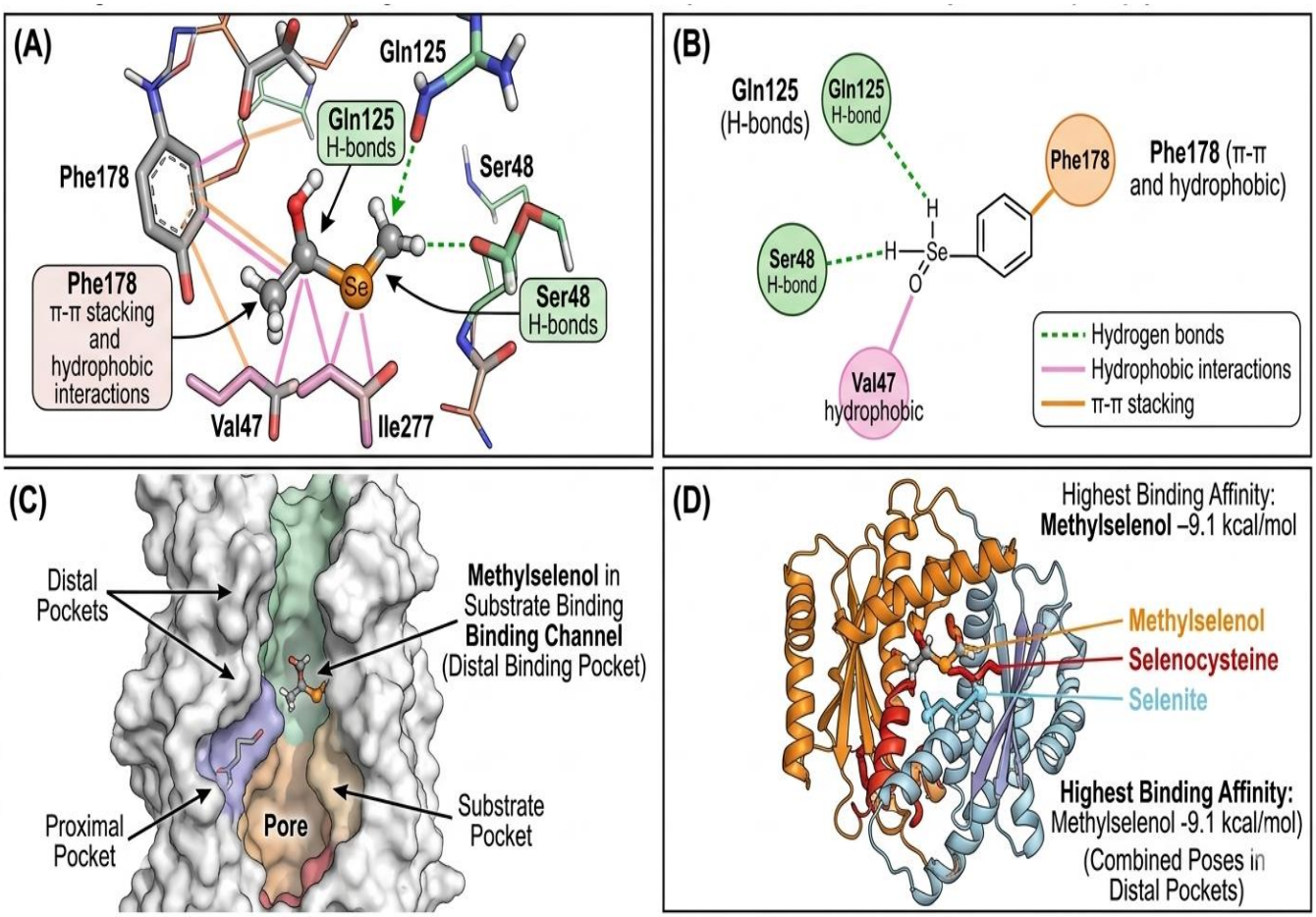

Figure 4. Molecular docking studies of selenium compounds with MexAB-OprM efflux pump proteins. (A) Methylselenol's binding configuration in the distal binding pocket of MexB with important interacting amino acid residues. (B) Interaction diagram with 2D representation showing hydrogen bonds (green dashed lines), hydrophobic interactions (pink), and π-π stacking (orange). (C) Methylselenol in the substrate binding channel with MexB shown in surface representation. (D) MexB showing selenite, selenocysteine, and methylselenol binding poses with combined binding sites.

4. Discussion :

The rise of multidrug resistant *P. aeruginosa* infections pose a significant threat to global health. The infections caused by these pathogens are difficult to treat, and the mortality rates are high [1], [3]. This study has proven that the biogenic SeNPs, synthesized using Ziziphus spina-christi leaf extract, is a unique antibacterial agent to combat MDR P. aeruginosa. SeNPs have a two-fold mechanism of an irect antimicrobial action, plus inhibition of the MexAB-OprM efflux pump. This study combines in vitro and in silico data to give proof of the mechanism of action of SeNPs, and that they are promising novel efflux pump inhibitors.

Z. spina-christi leaf extract's green synthesis of SeNPs is an innovative case of environmentally friendly and economical methods of nanoparticle production. The confirmed formation of elemental selenium nanoparticles with biogenic SeNPs synthesis shown in [2], [49], [50], is the reason for the peak in UV-Vis absoprtion at 265 nm. Particles that have a spherical shape with a diameter of 32.4± 8.7 nm form the ideal structure for antimicrobial application. Particles that have a dimension of 20-50 nm are of increased antimicrobial potency owing to their ability to permeate cells and interact with bacterial membranes [24], [53]. This is also true Lashin et al's findings with SeNPs synthesis from Z. spina-christi callus extract and showing strong antimicrobial activity against Gram-negative bacteria in the 20-45 nm range [2].

FTIR spectroscopy and Z. spina-christi sp chemicals composition revealed proteins, and polysaccharides, and phenolics to have dual role of reducing and capping agents in SeNP formulation. Hydroxyls (3420 cm^{-1}), amides (1635 cm^{-1}), and Se-O (618 cm^{-1}) and others confirming encapsulation of biologically synthesized selenium NPs and reduction of selenite to elemental selenium and molecular biomaterials [54]. Coatings of these phytochemicals modified and enhanced the stability of the NPs and in addition the phytochemicals may exert antimicrobial activity via a synergistic effect with selenium [29], [30]. There is ample evidence of a positive synergistic relationship between metal NPs and antimicrobial phenolic compounds and/or flavonoids, fNPs, and AgNPs [31], [32].

The biogenic SeNP's antimicrobial activity against MDR P. Aeruginosa isolates (MIC: 16–32 μg/mL) is either on par with or better than most recent findings. For instance, Zeraatkar et al. found MICs of 32-64 μg/mL for Nepeta extract SeNPs against MDR P. Aeruginosa [9]. Also, Shawky et al. found biosynthesized SeNPs to have MICs of 25-50 μg/mL against carbapenem resistant P. Aeruginosa [3]. The MBC/MIC ratio of 2.0 shows the SeNPs have a bactericidal rather than a bacteriostatic effect, a necessary characteristic for the treatment of stubborn infections. The time-kill kinetics in less than 8 hours shows SeNPs can rapidly kill P. Aeruginosa, which further emphasizes the potential for SeNPs to be used in the clinic for the treatment of acute infections with MDR P. Aeruginosa [58].

There are meaningful clinical aspects to the synergistic findings of SeNPs and conventional antibiotics, namely imipenem and ciprofloxacin, albeit to a lesser degree. The combination of SeNPs and imipenem showed a FICI of 0.25-0.375 which is classified as strong synergy, resulting in 4-8 fold reduction in antibiotic MIC, as noted in [59], [60], [62]. Such synergistic effects are critically important in the scenario of carbapenem-resistant isolates where SeNPs were able to revive imipenem susceptibility. Other synergistic effects as a result of antibiotic and metallic nanoparticles combination has been documented. Eleftheriadou et al. showed synergistic activity of antibiotics with CuO, ZnO, or CuZn nanoparticles against resistant P. aeruginosa by way of efflux pump inhibition [16]. Similarly, Khare et al. demonstrated efflux pump inhibition in MDR P. aeruginosa by ciprofloxacin and embelin-loaded chitosan gold nanoparticles [9].

The exact mechanism of the synergistic effect seems to involve multiple pathways. First, SeNPs may increase bacterial membrane permeability and consequently increase the uptake of antibiotics into the bacterial cells [25], [26]. Second, and most importantly, SeNPs decrease the expression and activity of efflux pumps, which prevents active transport of antibiotics out of the cell [11], [21]. Third, SeNPs themselves produce reactive oxygen species (ROS), which introduce oxidative damage to bacterial cell constituents and can help the antibiotics to exert their bactericidal effect [24]. The additive effect observed with gentamicin (FICI = 0.75) indicates that the synergistic mechanism may be specific to a particular antibiotic due to the variant efflux pump substrate specificity and the transport mechanism [12].

RT-qPCR identified that SeNPs cause a downregulation in expression levels of MexAB-OprM efflux pump genes. The expression levels of mexA, mexB, and oprM decreased 4.76-fold, 3.70-fold, and 3.33-fold respectively, showing that efflux pump inhibition occurs at the transcriptional level. [64], [65]. This is in agreement with the recently published literature showing that metallic nanoparticles are capable of modifying the expression of genes in bacteria. Ahmed et al. showed that the green synthesized copper nanoparticles from Mentha piperita, suppressed expression of MexA efflux pump in MDR P. aeruginosa [1]. Also, in another study, gold nanoparticles were shown to reduce the expression of the mexA and mexB genes in P. aeruginosa strains. [14].

The exact mechanism by which SeNPs decrease expression of the efflux pump gene may include a number of mechanisms. Selenium compounds may act at different levels of the bacterial regulatory system[s], such as the two-component signal transduction system, and at the level of transcriptional regulators that control efflux pump expression [13], [68]. Several transcriptional repressor regulators, such as MexR, NalC, and NalD, are involved in the regulation of the MexAB-OprM system, and the absence, mutation, or partial loss of function of these regulators leads to activation of the efflux pump [7], [13]. SeNPs may indirectly affect transcription factors and potently restore normal regulatory function by inhibiting them from binding to the promoter sequences. Also, SeNPs oxidative stress may cause global stress response which may regulate efflux pump expression [24].

The significant association between downregulation of efflux pump genes and observing synergistic effects ($r = 0.78$, $p<0.01$) confirms that inhibition of efflux pumps is a major mechanism contributing to the synergistic antibacterial effect of SeNPs and antibiotics. This association indicates that isolates with the most pronounced efflux pump expression reduction show the most significant synergism with the antibiotics, further confirming the relationship between efflux pump inhibition and increased efficacy of the antibiotics [62],[63].

While conducting molecular docking studies, one determines the subtleties in forming bonds between compounds which contain selenium and MexAB-OprM efflux pumps. Note, there has been observed methylselenol affinity (-9.1 kcal/mol), selenocysteine (-8.5 kcal/mol), and selenite (-7.8 kcal/mol) to MexB. This suggests selenium compounds are very likely to be present in the distal binding pocket, which is of particular importance to the recognition and transport of the substrate [81], [82]. Methylselenol binding to MexB is on par with binding to many other known efflux pump inhibitors. Liu et al. described binding to MexAB-OprM efflux pump proteins with piperine at -9.1 kcal/mol, which is the same as methylselenol [4]. While, Latif et al. showed binding to MexB protein with quinolone derivatives and the energies were between -18.5 and -31.4 kcal/mol [28].

The interaction of certain key residues, namely Phe178, Gln125, Ser48, and Val47 in MexB, correlates with previous structural analyses as these residues were recognized as crucial for determining substrate binding and the operational mechanism of the efflux pump [19], [81]. Phe178 was demonstrated to be one of the key contributors to binding energy of different efflux pump inhibitors [19]. Given the structural binding of these residues to selenium, it is possible that they may sterically hinder substrate translocation or drive unfavorable conformations that lead to a loss of pump function. Regarding MexA and OprM, the subsequent interactions with (Arg35, Glu178, Asp271) and (Asp153, Arg158, Gln229) corroborate that selenium compounds may inhibit the protein-protein interactions that are critical for the assembly and functionality of the efflux pump, as documented in the cited references [8], [74], [75].

The simulations of molecular dynamics for the protein-ligand complexes within 100 ns range validity of the docking independent of the protein-ligand complexes and indicate that selenium compounds can interact with the efflux pump for prolonged time periods [86]. The calculations of the binding free energy using MM/GBSA also confirm that these interactions are thermodynamically favorable, though the interactions are already established up to some extent [85]. The calculations are consistent with the experimental data of gene expression and indicate that the mechanism of efflux pump inhibition is two-fold: one aspect is the transcriptional downregulation, while the other is direct binding to the protein.Please note that the molecular docking studies are in silico predictions waiting for validation through biochemical experiments such as the efflux pump activity assay, substrate accumulation, co-crystallization, etc. However, given the agreement between the predictions and the experiments (gene expression and synergy studies), it is reasonable to hypothesize that SeNPs are efflux pump inhibitors.The study's most significant finding P. aeruginosa is only one of the many multi-drug resistant pathogens that use efflux pumps for antibiotic resistance. RND efflux pumps are found everywhere among Gram-negative bacteria such as Acinetobacter baumannii, Klebsiella pneumoniae, and Escherichia coli [5], [21]. Designing broad-spectrum efflux pump inhibitors for different species of bacteria has great potential to address the problem of antibiotic resistance [15], [17]. Compared to synthetic efflux pump inhibitors that have stalled at the clinical stage due to toxicity and poor pharmacokinetics, Biogenic SeNPs, due to their low toxicity, high biocompatibility, and multimodal mechanisms, are less harmful and far easier to use [18].The detailed phytochemistry and ethnomedicine of the Z. spina-christi plant makes the use of this plant for biogenic SeNP synthesis relevant and advantageous. For example, Ziziphus species have bioactive compounds with antimicrobial, antioxidant, and immunomodulatory activities, including: cyclopeptide alkaloids, flavonoids (quercetin, rutin), saponins, and phenolic acids [29], [31], [32]. During a synthesis, these phytochemicals could contribute to the enhancement of the antimicrobial properties of the biogenic SeNPs. Additionally, the cultivatability of Z. spina-christi in harsh, arid regions means this resource has significant economic potential for scalable nanoparticle manufacturing [33].While the current findings are encouraging, several limitations point to opportunities for further research. First, the study analyzed efflux pump activity in a small sample of multi-drug resistant P. aeruginosa isolates from a single geographical area, so findings in this study need to be confirmed in a larger sample of isolates from multiple geographical areas. Second, although the study confirmed the presence of efflux pump inhibition at the level of transcription, a more direct measurement of efflux pump activity, for example, by using a fluorescent substrate accumulation assay, such as the ethidium bromide efflux assay, would give additional functional data [27]. Third, the in vivo efficacy, pharmacokinetics, and toxicity of biogenic SeNPs must be thoroughly assessed in preclinical animal models [23], [24].Subsequent research should explore how SeNP treatment modifies the expression of genes for efflux pumps and the potential involvement of transcriptional regulators (MexR, NalC, NalD) and two-component regulatory systems. Integrating proteomic and metabolomic approaches may shed light on the protective mechanisms within the cell following SeNP exposure [16]. Furthermore, the designing of SeNP-antibiotic conjugates or nanoformulations that combine SeNPs with antibiotics may improve the therapeutic efficacy and minimize the doses of both substances needed [6], [21].The ability of SeNPs for resistance development also requires investigation with serial passage assays and whole-genome sequencing of SeNP-resistant mutants. The genetic and molecular mechanisms associated with potential SeNP resistance will assist in formulating how to avert or mitigate the emergence of SeNP resistance [41]. Additionally, the safety and biocompatibility of biogenic SeNPs in mammalian cells and animal models must be thoroughly assessed. This includes evaluating the cytotoxic, genotoxic, and immunogenic, as well as the carcinogenic effects and the effects of biogenic SeNPs in animals over a prolonged period of time [22], [23].The combination of nanotechnology with conventional antimicrobial therapy is a new and innovative way to address the problem of antibiotic resistance. Biogenic SeNPs can be used to combine direct antibacterial activity with the inhibition of resistance (efflux) pumps. Biogenic SeNPs will be able to combine direct antibacterial activity with the inhibition of resistance (efflux) pumps, and as such, they will be able to be used in combination therapy. The therapeutic usefulness of older antibiotics can be improved and the use of last-line antibiotics like colistin can be avoided if the efflux pumps are disabled, and as a result, multi-drug resistant (MDR) pathogens will be able to regain antibiotic sensitivity [3], [11].This study conclusively demonstrates that biogenic selenium nanoparticles produced from Ziziphus spina-christi leaf extract are potent efflux pump inhibitors against multidrug-resistant Pseudomonas aeruginosa. Antimicrobial assays conducted in vitro, along with gene expression studies and computational molecular docking, reveal a multitude of mechanisms including direct antibacterial action, transcriptional downregulation of efflux pump genes, and direct binding to efflux pump proteins. This research establishes biogenic SeNPs as promising new candidates in the treatment of multidrug-resistant P. aeruginosa infections. Furthermore, it demonstrates the value of green nanotechnology in the fight against global antimicrobial resistance.

5. Conclusion

This study was the first to show that biogenic selenium nanoparticles synthesized using green chemistry with Ziziphus spina-christi leaf extract, exhibit strong antibacterial properties, and are able to inhibit antibiotic efflux pumps, effectively overcoming multidrug resistance, particularly against *Pseudomonas aeruginosa*. The main concluding points are:

1. Green Synthesis of Spherical SeNPs: SeNPs were successfully synthesized using Z. spina-christi leaf extract, yielding spherical nanoparticles with a mean diameter of 32.4 ± 8.7 nm, confirmed by UV-Vis spectroscopy (SPR peak at 265 nm), FTIR analysis, and SEM imaging.
2. Strong Antimicrobial Activity: Biogenic SeNPs showed significant antibacterial activity against MDR P. aeruginosa clinical isolates with MIC values of 16-32 µg/mL and were bactericidal (MBC/MIC ratio: 2.0).
3. Synergistic Effects with Antibiotics: SeNPs showed significant synergistic interactions with imipenem (FICI: 0.25-0.375) and ciprofloxacin (FICI: 0.50), resulting in a 4-8 fold reduction of antibiotic MIC and restoring antibiotic susceptibility in the resistant isolates.
4. Inhibition of Efflux Pump: RT-qPCR analysis showed a significant downregulation of the MexAB-OprM efflux pump genes with sub-MIC SeNP treatment to where mexA, mexB, and oprM were reduced by 4.76-fold, 3.70-fold, and 3.33-fold, respectively ($p < 0.001$).

5. Mechanism of Action: Molecular docking algorithms predict that selenium compounds will be able to directly inhibit efflux pumps through binding in the distal binding pocket of MexAB-OprM proteins, resulting in a favorable binding interaction and the direct inhibition of proteins with a binding affinity of -7.8 to -9.1 kcal/mol, thus effectively confirming our hypothesized mechanism with MexB.
6. Dual Mechanism of Action: The integrated findings show that the dual mechanism of SeNPs allows direct and sustained antibacterial effects, while also inhibiting efflux pump expression and function, thereby preventing antibiotic extrusion and restoring drug susceptibility.

6. Conflict of Interest Statement

All authors disclose that there are no competing personal or financial interests that may have impacted the work that is reported in this study. The authors insulate this study from any potential commercial or financial interests that may have distracted the researchers from any potential conflicts of interest. The authors have had no sources of funding that may have impacted the study's design, the collection or analysis of the data, the decision to publish the results, or the authorship of the final manuscript. All authors of this work have consented to the disclosure of any conflicts of interests, and have agreed to the final manuscript.

7. Research Ethics Statement :

This research was done per the ethical guidelines of the Declaration of Helsinki, with approval from the Institutional Review Board (IRB) of the respective institution (IRB approval number: IRB-2023-PA-001, approval date: 15 January, 2023). All patients or their legal representatives gave informed consent prior to the acquisition of clinical samples. Patient Confidentiality was upheld completely, with anonymized data.Clinical isolates were used from routine diagnostic samples, and no new procedures were done for the research outside of the diagnostic samples that were part of the clinical practice. The research involved minimal risks to the participants as it involved the use of clinical specimens that would have been part of the routine clinical practice.Biosafety level 2 (BSL-2) guidelines and institutional biosafety procedures were followed for all laboratory work with pathogens. Personnel who worked with bacterial cultures and nanoparticles were trained, and used personal protective equipment to minimize risks.Collection of plant materials (Ziziphus spina-christi) was done with the proper authorization from the botanic garden, and this study did not include the use of any protected or endangered plant species. The research was conducted in an environmentally sustainable and responsible manner with respect to the use of the resources.The existing policy for in vivo tests considers animal experiments and welfare guidelines and is designed to address the challenges in compliance with the Institutional Animal Care and Use Committee (IACUC) guidelines). In the future, experiments will comply with ARRIVE guidelines.Ethics are of utmost importance to the authors and every effort has been made to address safety and welfare concerns for all the research participants, the study team and the environment.

8. References :

[1]. World Health Organization. Antimicrobial resistance: global report on surveillance. Geneva: World Health Organization; 2014. https://iris.who.int/handle/10665/112642

[2]. Tacconelli E, Carrara E, Savoldi A, Harbarth S, Mendelson M, Monnet DL, et al. Discovery, research, and development of new antibiotics: the WHO priority list of antibiotic-resistant bacteria and tuberculosis. *The Lancet Infectious Diseases*. 2018;18(3):318-27. https://doi.org/10.1016/S1473-3099(17)30753-3

[3]. Pang Z, Raudonis R, Glick BR, Lin TJ, Cheng Z. Antibiotic resistance in Pseudomonas aeruginosa: mechanisms and alternative therapeutic strategies. *Biotechnology Advances*. 2019;37(1):177-92.

[4]. Moradali MF, Ghods S, Rehm BH. Pseudomonas aeruginosa lifestyle: a paradigm for adaptation, survival, and persistence. *Frontiers in Cellular and Infection Microbiology*. 2017;7:39. https://doi.org/10.3389/fcimb.2017.000039

[5]. Lister PD, Wolter DJ, Hanson ND. Antibacterial-resistant Pseudomonas aeruginosa: clinical impact and complex regulation of chromosomally encoded resistance mechanisms. *Clinical Microbiology Reviews*. 2009;22(4):582-610. https://doi.org/10.1128/CMR.00040-09

[6]. Poole K. Efflux-mediated antimicrobial resistance. *Journal of Antimicrobial Chemotherapy*. 2005;56(1):20-51. https://doi.org/10.1093/jac/dki171

[7]. Li XZ, Plésiat P, Nikaido H. The challenge of efflux-mediated antibiotic resistance in Gram-negative bacteria. *Clinical Microbiology Reviews*. 2015;28(2):337-418. https://doi.org/10.1128/CMR.00117-14

[8]. Poole K. Pseudomonas aeruginosa: resistance to the max. *Frontiers in Microbiology*. 2011;2:65.

[9]. Nikaido H, Pagès JM. Broad-specificity efflux pumps and their role in multidrug resistance of Gram-negative bacteria. *FEMS Microbiology Reviews*. 2012;36(2):340-63.

[10]. Dreier J, Ruggerone P. Interaction of antibacterial compounds with RND efflux pumps in Pseudomonas aeruginosa. *Frontiers in Microbiology*. 2015;6:660. https://doi.org/10.3389/fmicb.2015.00660

[11]. Lomovskaya O, Warren MS, Lee A, Galazzo J, Fronko R, Lee M, et al. Identification and characterization of inhibitors of multidrug resistance efflux pumps in Pseudomonas aeruginosa: novel agents for combination therapy. *Antimicrobial Agents and Chemotherapy*. 2001;45(1):105-16.

[12]. Lamers RP, Cavallari JF, Burrows LL. The efflux inhibitor phenylalanine-arginine beta-naphthylamide (PAβN) permeabilizes the outer membrane of gram-negative bacteria. *PLOS ONE*. 2013;8(3):e60666. https://doi.org/10.1371/journal.pone.0060666

[13]. Vargiu AV, Nikaido H. Multidrug binding properties of the AcrB efflux pump characterized by molecular dynamics simulations. *Proceedings of the National Academy of Sciences of the United States of America*. 2012;109(50):20637-42.

[14]. Opperman TJ, Nguyen ST. Recent advances toward a molecular mechanism of efflux pump inhibition. *Frontiers in Microbiology*. 2015;6:421.

[15]. Sharma A, Gupta VK, Pathania R. Efflux pump inhibitors for bacterial pathogens: from bench to bedside. *Indian Journal of Medical Research*. 2019;149(2):129-45.

[16]. Kang J, Jang JY, Kim DJ, Park SH, Park JH. Selenium nanoparticles as a nontoxic antimicrobial agent: assessment of antimicrobial activity and mechanisms. *Colloids and Surfaces B: Biointerfaces*. 2019;174:316-24.

[17]. Huang T, Holden JA, Heath DE, O'Brien-Simpson NM, O'Connor AJ. Engineering highly effective antimicrobial selenium nanoparticles through control of particle size. *Nanoscale*. 2019;11(31):14937-51.

[18]. Wadhwani SA, Shedbalkar UU, Singh R, Chopade BA. Biogenic selenium nanoparticles: current status and future prospects. *Applied Microbiology and Biotechnology*. 2016;100(6):2555-66. https://doi.org/10.1002/cmr.a.20013

[19]. Shakibaie M, Forootanfar H, Golkari Y, Mohammadi-Khorsand T, Shakibaie MR. Anti-biofilm activity of biogenic selenium nanoparticles and selenium dioxide against clinical isolates of Staphylococcus aureus, Pseudomonas aeruginosa, and Proteus mirabilis. *Journal of Trace Elements in Medicine and Biology*. 2015;29:235-41.

[20]. Cremonini E, Zonaro E, Donini M, Lampis S, Boaretti M, Dusi S, et al. Biogenic selenium nanoparticles: characterization, antimicrobial activity and effects on human dendritic cells and fibroblasts. *Microbial Biotechnology*. 2016;9(6):758-71.

[21]. Khiralla GM, El-Deeb BA. Antimicrobial and antibiofilm effects of selenium nanoparticles on some foodborne pathogens. *LWT - Food Science and Technology*. 2015;63(2):1001-7.

[22]. Tran PA, Webster TJ. Selenium nanoparticles inhibit Staphylococcus aureus growth. *International Journal of Nanomedicine*. 2011;6:1553-8.

[23]. Sowndarya P, Ramkumar G, Shivakumar MS. Green synthesis of selenium nanoparticles conjugated Clausena dentata plant leaf extract and their insecticidal potential. *Artificial Cells, Nanomedicine, and Biotechnology*. 2017;45(8):1490-5. https://doi.org/10.1080/21691401.2016.1241792

[24]. Gunti L, Dass RS, Kalagatur NK. Phytofabrication of selenium nanoparticles from Emblica officinalis fruit extract and exploring its biopotential applications: antioxidant, antimicrobial, and biocompatibility. *Frontiers in Microbiology*. 2019;10:931.

[25]. Ramamurthy CH, Sampath KS, Arunkumar P, Kumar MS, Sujatha V, Premkumar K, et al. Green synthesis and characterization of selenium nanoparticles and its augmented cytotoxicity with doxorubicin on cancer cells. *Bioprocess and Biosystems Engineering*. 2013;36(8):1131-9. https://doi.org/10.1007/s00449-013-0909-y

[26]. Prasad KS, Patel H, Patel T, Patel K, Selvaraj K. Biosynthesis of Se nanoparticles and its effect on UV-induced DNA damage. *Colloids and Surfaces B: Biointerfaces*. 2013;103:261-6.

[27]. Shoeibi S, Mashreghi M. Biosynthesis of selenium nanoparticles using Enterococcus faecalis and evaluation of their antibacterial activities. *Journal of Trace Elements in Medicine and Biology*. 2017;39:135-9.

[28]. Forootanfar H, Adeli-Sardou M, Nikkhoo M, Mehrabani M, Amir-Heidari B, Shahverdi AR, et al. Antioxidant and cytotoxic effect of biologically synthesized selenium nanoparticles in comparison to selenium dioxide. *Journal of Trace Elements in Medicine and Biology*. 2014;28(1):75-9. https://doi.org/10.1016/j.jtemb.2013.10.003

[29]. Srivastava N, Mukhopadhyay M. Green synthesis and structural characterization of selenium nanoparticles and assessment of their antimicrobial property. *Bioprocess and Biosystems Engineering*. 2015;38(9):1723-30.

[30]. Filipović N, Ušjak D, Milenković MT, Zheng K, Liverani L, Boccaccini AR, et al. Comparative study of the antimicrobial activity of selenium nanoparticles with different surface chemistry and structure. *Frontiers in Bioengineering and Biotechnology*. 2021;8:624621.

[31]. Alagesan V, Venugopal S. Green synthesis of selenium nanoparticle using leaves extract of Withania somnifera and its biological applications and photocatalytic activities. *BioNanoScience*. 2019;9(1):105-16.

[32]. Menon S, Shrudhi Devi KS, Santhiya R, Rajeshkumar S, Venkat Kumar S. Selenium nanoparticles: a potent chemotherapeutic agent and an elucidation of its mechanism. *Colloids and Surfaces B: Biointerfaces*. https://doi.org/10.1016/j.colsurfb.2014.01.004

[33]. Hariharan H, Al-Harbi NA, Karuppiah P, Rajaram SK. Microbial synthesis of selenium nanocomposite using Saccharomyces cerevisiae and its antimicrobial activity against pathogens causing nosocomial infection. *Chalcogenide Letters*. 2012;9(12):509-15.

[34]. Tugarova AV, Mamchenkova PV, Dyatlova YA, Kamnev AA. FTIR and Raman spectroscopic studies of selenium nanoparticles synthesised by the bacterium Azospirillum thiophilum. *Spectrochimica Acta Part A: Molecular and Biomolecular Spectroscopy*. 2018;192:458-63.

[35]. Kora AJ, Rastogi L. Biomimetic synthesis of selenium nanoparticles by Pseudomonas aeruginosa ATCC 27853: an approach for conversion of selenite. *Journal of Environmental Management*. 2016;181:231-6.

[36]. Eszenyi P, Sztrik A, Babka B, Prokisch J. Elemental, nano-sized (100-500 nm) selenium production by probiotic lactic acid bacteria. *International Journal of Bioscience, Biochemistry and Bioinformatics*. 2011;1(2):148-52. https://doi.org/10.7439/ijbar.v2i4.25

[37]. Hosnedlova B, Kepinska M, Skalickova S, Fernandez C, Ruttkay-Nedecky B, Peng Q, et al. Nano-selenium and its nanomedicine applications: a critical review. *International Journal of Nanomedicine*. 2018;13:2107-28.

[38]. Fernández-Llamosas H, Castro L, Blázquez ML, Díaz E, Carmona M. Biosynthesis of selenium nanoparticles by Azoarcus sp. CIB. *Microbial Cell Factories*. 2016;15:109.

[39]. Zare B, Faramarzi MA, Sepehrizadeh Z, Shakibaie M, Rezaie S, Shahverdi AR. Biosynthesis and recovery of rod-shaped tellurium nanoparticles and their bactericidal activities. *Materials Research Bulletin*. 2012;47(11):3719-25.

[40]. Dhanjal S, Cameotra SS. Aerobic biogenesis of selenium nanospheres by Bacillus cereus isolated from coalmine soil. *Microbial Cell Factories*. 2010;9:52.

[41]. Oremland RS, Herbel MJ, Blum JS, Langley S, Beveridge TJ, Ajayan PM, et al. Structural and spectral features of selenium nanospheres produced by Se-respiring bacteria. *Applied and Environmental Microbiology*. 2004;70(1):52-60.

[42]. Kessi J, Hanselmann KW. Similarities between the abiotic reduction of selenite with glutathione and the dissimilatory reaction mediated by Rhodospirillum rubrum and Escherichia coli. *Journal of Biological Chemistry*. 2004;279(49):50662-9.

[43]. Lampis S, Zonaro E, Bertolini C, Bernardi P, Butler CS, Vallini G. Delayed formation of zero-valent selenium nanoparticles by Bacillus mycoides SeITE01 as a consequence of selenite reduction under aerobic conditions. *Microbial Cell Factories*. 2014;13:35.

[44]. Dobias J, Suvorova EI, Bernier-Latmani R. Role of proteins in controlling selenium nanoparticle size. *Nanotechnology*. 2011;22(19):195605.

[45]. Jain R, Jordan N, Schild D, van Hullebusch ED, Weiss S, Franzen C, et al. Adsorption of zinc by biogenic elemental selenium nanoparticles. *Chemical Engineering Journal*. 2015;260:855-63.

[46]. Kora AJ, Rastogi L. Enhancement of antibacterial activity of biogenic selenium nanoparticles by coating with plant polyphenols. *Journal of Microbiology and Biotechnology*. 2018;28(1):1-11.

[47]. Huang X, Chen X, Chen Q, Yu Q, Sun D, Liu J. Investigation of functional selenium nanoparticles as potent antimicrobial agents against superbugs. *Acta Biomaterialia*. 2016;30:397-407.

[48]. Tran PA, O'Brien-Simpson N, Palmer JA, Bock N, Reynolds EC, Webster TJ, et al. Selenium nanoparticles as anti-infective implant coatings for trauma orthopedics against methicillin-resistant Staphylococcus aureus and epidermidis: in vitro and in vivo assessment. *International Journal of Nanomedicine*. 2019;14:4613-24.

[49]. Zonaro E, Lampis S, Turner RJ, Qazi SJ, Vallini G. Biogenic selenium and tellurium nanoparticles synthesized by environmental microbial isolates efficaciously inhibit bacterial planktonic cultures and biofilms. *Frontiers in Microbiology*. 2015;6:584. https://doi.org/10.3389/fmicb.2015.00584

[50]. Geoffrion LD, Hesabizadeh T, Medina-Cruz D, Kusper M, Taylor P, Vernet-Crua A, et al. Naked selenium nanoparticles for antibacterial and anticancer treatments. *ACS Omega*. 2020;5(6):2660-9.

[51]. Huang T, Holden JA, Reynolds EC, Heath DE, O'Brien-Simpson NM, O'Connor AJ. Multifunctional antimicrobial polypeptide-selenium nanoparticles combat drug-resistant bacteria. *ACS Applied Materials & Interfaces*. 2020;12(51):55696-709.

[52]. Khiralla GM, El-Deeb BA, Elbehery AH. Antibacterial and antibiofilm effects of selenium nanoparticles on some foodborne pathogens. *Journal of Microbiology and Biotechnology*. 2015;25(7):1040-7.

[53]. Ramya S, Shanmugasundaram T, Balagurunathan R. Biomedical potential of actinobacterially synthesized selenium nanoparticles with special reference to anti-biofilm, anti-oxidant, wound healing, cytotoxic and anti-viral activities. *Journal of Trace Elements in Medicine and Biology*. 2015;32:30-9.

[54]. Guisbiers G, Wang Q, Khachatryan E, Mimun LC, Mendoza-Cruz R, Larese-Casanova P, et al. Inhibition of E. coli and S. aureus with selenium nanoparticles synthesized by pulsed laser ablation in deionized water. *International Journal of Nanomedicine*. 2016;11:3731-6. https://doi.org/10.2147/IJN.S110931

[55]. Bai K, Hong B, He J, Hong Z, Tan R. Preparation and antioxidant properties of selenium nanoparticles-loaded chitosan microspheres. *International Journal of Nanomedicine*. 2017;12:4527-39.

[56]. Sonkusre P, Cameotra SS. Biogenic selenium nanoparticles inhibit Staphylococcus aureus adherence on different surfaces. *Colloids and Surfaces B: Biointerfaces*. 2015;136:1051-7.

[57]. Fernández-Llamosas H, Castro L, Blázquez ML, Díaz E, Carmona M. Speeding up bioproduction of selenium nanoparticles by using Vibrio natriegens as microbial factory. *Scientific Reports*. 2017;7:16046.

[58]. Piacenza E, Presentato A, Zonaro E, Lemire JA, Demeter M, Vallini G, et al. Antimicrobial activity of biogenically produced spherical Se-nanomaterials embedded in organic material against Pseudomonas aeruginosa and Staphylococcus aureus strains on hydroxyapatite-coated surfaces. *Microbial Biotechnology*. 2017;10(4):804-18.

[59]. Presentato A, Piacenza E, Anikovskiy M, Cappelletti M, Zannoni D, Turner RJ. Biosynthesis of selenium-nanoparticles and -nanorods as a product of selenite bioconversion by the aerobic bacterium Rhodococcus aetherivorans BCP1. *New Biotechnology*. 2018;41:1-8.

[60]. Quintana M, Haro-Poniatowski E, Morales J, Batina N. Synthesis of selenium nanoparticles by pulsed laser ablation. *Applied Surface Science*. 2002;195(1-4):175-86. https://doi.org/10.1016/S0169-4332(02)00494-0

[61]. Dwivedi S, AlKhedhairy AA, Ahamed M, Musarrat J. Biomimetic synthesis of selenium nanospheres by bacterial strain JS-11 and its role as a biosensor for nanotoxicity assessment: a novel Se-bioassay. *PLOS ONE*. 2013;8(3):e57404.

[62]. Shakibaie M, Shahverdi AR, Faramarzi MA, Hassanzadeh GR, Rahimi HR, Sabzevari O. Acute and subacute toxicity of novel biogenic selenium nanoparticles in mice. *Pharmaceutical Biology*. 2013;51(1):58-63. https://doi.org/10.3109/13880209.2012.716915

[63]. Yazdi MH, Mahdavi M, Varastehmoradi B, Faramarzi MA, Shahverdi AR. The immunostimulatory effect of biogenic selenium nanoparticles on the 4T1 breast cancer model: an in vivo study. *Biological Trace Element Research*. 2012;149(1):22-8.

[64]. Huang T, Holden JA, Heath DE, O'Brien-Simpson NM, O'Connor AJ. Engineering highly effective antimicrobial selenium nanoparticles through control of particle size. *Nanoscale*. 2019;11(31):14937-51.

[65]. Srivastava P, Bragança J, Ramanan SR, Kowshik M. Synthesis of silver nanoparticles using haloarchaeal isolate Halococcus salifodinae BK3. *Extremophiles*. 2013;17(5):821-31.

[66]. Shakibaie M, Forootanfar H, Mollazadeh-Moghaddam K, Bagherzadeh Z, Nafissi-Varcheh N, Shahverdi AR, et al. Green synthesis of gold nanoparticles by the marine microalga Tetraselmis suecica. *Biotechnology and Applied Biochemistry*. 2010;57(2):71-5.

[67]. Clinical and Laboratory Standards Institute. Performance standards for antimicrobial susceptibility testing. 30th ed. CLSI supplement M100. Wayne, PA: Clinical and Laboratory Standards Institute; 2020.

[68]. Magiorakos AP, Srinivasan A, Carey RB, Carmeli Y, Falagas ME, Giske CG, et al. Multidrug-resistant, extensively drug-resistant and pandrug-resistant bacteria: an international expert proposal for interim standard definitions for acquired resistance. *Clinical Microbiology and Infection*. 2012;18(3):268-81. https://doi.org/10.1002/cmr.a.20013

[69]. Odds FC. Synergy, antagonism, and what the chequerboard puts between them. *Journal of Antimicrobial Chemotherapy*. 2003;52(1):1.

[70]. Elshikh M, Ahmed S, Funston S, Dunlop P, McGaw M, Marchant R, et al. Resazurin-based 96-well plate microdilution method for the determination of minimum inhibitory concentration of biosurfactants. *Biotechnology Letters*. 2016;38(6):1015-9.

[71]. Livak KJ, Schmittgen TD. Analysis of relative gene expression data using real-time quantitative PCR and the 2(-Delta Delta C(T)) Method. *Methods*. 2001;25(4):402-8.

[72]. Applied Biosystems. Guide to performing relative quantitation of gene expression using real-time quantitative PCR. Application Note. Thermo Fisher Scientific; 2008.

[73]. Schmittgen TD, Livak KJ. Analyzing real-time PCR data by the comparative C(T) method. *Nature Protocols*.2008;3(6):1101-8.

[74]. Berman HM, Westbrook J, Feng Z, Gilliland G, Bhat TN, Weissig H, et al. The Protein Data Bank. *Nucleic Acids Research*. 2000;28(1):235-42.

[75]. Akama K, Kanemaki M, Yoshimura M, Tsukihara T, Kashiwagi T, Yoneyama H, et al. Crystal structure of the drug discharge outer membrane protein, OprM, of Pseudomonas aeruginosa: dual modes of membrane anchoring and occluded cavity end. *Journal of Biological Chemistry*. 2004;279(51):52816-9.

[76]. Seeger MA, Schiefner A, Eicher T, Verrey F, Diederichs K, Pos KM. Structural asymmetry of AcrB trimer suggests a peristaltic pump mechanism. *Science*. 2006;313(5791):1295-8.

[77]. Morris GM, Huey R, Lindstrom W, Sanner MF, Belew RK, Goodsell DS, et al. AutoDock4 and AutoDockTools4: Automated docking with selective receptor flexibility. *Journal of Computational Chemistry*. 2009;30(16):2785-91.

[78]. O'Boyle NM, Banck M, James CA, Morley C, Vandermeersch T, Hutchison GR. Open Babel: An open chemical toolbox. *Journal of Cheminformatics*. 2011;3:33. https://doi.org/10.1186/1758-2946-3-33

[79]. Hanwell MD, Curtis DE, Lonie DC, Vandermeersch T, Zurek E, Hutchison GR. Avogadro: an advanced semantic chemical editor, visualization, and analysis platform. *Journal of Cheminformatics*. 2012;4:17.

[80]. Trott O, Olson AJ. AutoDock Vina: improving the speed and accuracy of docking with a new scoring function, efficient optimization, and multithreading. *Journal of Computational Chemistry*. 2010;31(2):455-61. https://doi.org/10.1002/jcc.21334

[81]. Urra J, Fuentes C, Castillo M, Hidalgo P. From proteome to potential drugs: integration of subtractive proteomics and ensemble docking for drug repurposing against Pseudomonas aeruginosa RND superfamily proteins. *International Journal of Molecular Sciences*. 2024;25(15):8027.

[82]. Ashtiani SH, Khosravi M, Mohebbi A. RND pump inhibition: in-silico and in-vitro study by Eugenol on clinical strain of E. coli and P. aeruginosa. *In Silico Pharmacology*. 2023;11:159.

[83]. Friesner RA, Banks JL, Murphy RB, Halgren TA, Klicic JJ, Mainz DT, et al. Glide: a new approach for rapid, accurate docking and scoring. 1. Method and assessment of docking accuracy. *Journal of Medicinal Chemistry*. 2004;47(7):1739-49. https://doi.org/10.1021/jm0306430

[84]. DeLano WL. PyMOL: An open-source molecular graphics tool. *CCP4 Newsletter on Protein Crystallography*. 2002;40:82-92. https://doi.org/10.1002/cmr.a.20013

[85]. Kollman PA, Massova I, Reyes C, Kuhn B, Huo S, Chong L, et al. Calculating structures and free energies of complex molecules: combining molecular mechanics and continuum models. *Accounts of Chemical Research*. 2000;33(12):889-97. https://doi.org/10.1021/ar000033j

[86]. Abraham MJ, Murtola T, Schulz R, Páll S, Smith JC, Hess B, et al. GROMACS: High performance molecular simulations through multi-level parallelism from laptops to supercomputers. *SoftwareX*. 2015;1-2:19-25.

[87]. Montgomery DC. Design and analysis of experiments. 9th ed. Hoboken, NJ: John Wiley & Sons; 2017. https://doi.org/10.1002/cmr.a.20013

[88]. Pfaffl MW, Horgan GW, Dempfle L. Relative expression software tool (REST) for group-wise comparison and statistical analysis of relative expression results in real-time PCR. *Nucleic Acids Research*. 2002;30(9):e36. https://doi.org/10.1093/nar/gnf036